Title

Magnetism and Mössbauer study of formation of multi-core γ - Fe 2 O 3 nanoparticles

Authors

Kamali, Saeed
Bringas, Eugenio
Hah, Hien-Yoong
et al.

Publication Date

2018-04-01

DOI

10.1016/j.jmmm.2017.10.102

Peer reviewed

Journal of Magnetism and Magnetic Materials 451 (2018) 131–136

Contents lists available at ScienceDirect

Journal of Magnetism and Magnetic Materials

journal homepage: www.elsevier.com/locate/jmmm

Research articles

Magnetism and Mössbauer study of formation of multi-core γ-Fe_2O_3 nanoparticles

Saeed Kamali [a,*], Eugenio Bringas [b], Hien-Yoong Hah [a], Brian Bates [c], Jacqueline A. Johnson [a], Charles E. Johnson [d], Pieter Stroeve [e]

[a] Department of Mechanical, Aerospace and Biomedical Engineering, University of Tennessee Space Institute, Tullahoma, TN 37388, United States
[b] Department of Chemical and Biomolecular Engineering, University of Cantabria, Av. de los Castros s/n, 39005 Santander, Cantabria, Spain
[c] Center for Manufacturing Research, Tennessee Technological University, Cookeville, TN 38505, United States
[d] Center for Laser Applications, University of Tennessee Space Institute, Tullahoma, TN 37388, United States
[e] Department of Chemical Engineering, University of California Davis, Davis, CA 95616, United States

ARTICLE INFO

Article history:
Received 7 June 2017
Received in revised form 17 September 2017
Accepted 25 October 2017
Available online 26 October 2017

Keywords:
Multi-core-shell nanoparticles
Maghemite nanoparticles
Mössbauer spectroscopy
High-resolution transmission electron microscopy
Magnetization measurements
Nanomagnetism

ABSTRACT

A systematic investigation of magnetic nanoparticles and the formation of a core-shell structure, consisting of multiple maghemite (γ-Fe_2O_3) nanoparticles as the core and silica as the shell, has been performed using various techniques. High-resolution transmission electron microscopy clearly shows isolated maghemite nanoparticles with an average diameter of 13 nm and the formation of a core-shell structure. Low temperature Mössbauer spectroscopy reveals the presence of pure maghemite nanoparticles with all vacancies at the B-sites. Isothermal magnetization and zero-field-cooled and field-cooled measurements are used for investigating the magnetic properties of the nanoparticles. The magnetization results are in good accordance with the contents of the magnetic core and the non-magnetic shell. The multiple-core γ-Fe_2O_3 nanoparticles show similar behavior to isolated particles of the same size.

1. Introduction

An important class of nanostructures is magnetic nanocrystallites which have a wide range of applications in numerous fields, ranging from new functional materials [1] such as magnetic recording media [2] to biomedical diagnostics and therapy [3] such as cancer treatment by hyperthermia [4], magnetic resonance imaging (MRI), and drug delivery [5]. Iron-oxide nanocrystallites are the most interesting and studied systems in this class of materials. The abundance, stability, and very high saturation magnetic moments make many of the iron-oxides very good components for technological applications.

Small iron-oxide nanoparticles, below 100 nm, are magnetic single domains resulting in large magnetic moments, Nμ, with N as the number of atoms in the particle and μ as the magnetic moment of each atom. Moreover, iron-oxide nanoparticles, around 10 nm or smaller, possess superparamagnetism [6–8], which is an important feature in hyperthermia, a revolutionary step in medicine [9,4]. In this process ferromagnetic or ferrimagnetic nanoparticles of iron oxides are used to promote cell necrosis using controlled local heating of tissue, where magnetic nanoparticles coated with a lipid bilayer, magnetoliposomes, are used. To obtain the maximum heat transfer for the lowest possible field-strength and magnetoliposome concentration, the magnetoliposome size, core-material size, and AC frequency have to be optimized.

Chemical functionality and drug delivery for synergetic medical treatments, using magnetic nanoparticles coated in lipid bilayers [10,11] are other examples. The delivery of different kinds of drugs to the cell membrane with nanoparticles is described elsewhere [12–14].

Furthermore, the chemical and physical stimuli-responsive gated mesoporous materials can be designed to function as smart nanodevices. High homogeneous porosity, thermal stability, inertness, robustness, the presence of tunable pore sizes, and high loading capacity, make functionalized mesoporous silica an ideal compound for hosting functional guest molecules. Incorporating external surface functional groups opening or closing pores at will or including capping molecules, make it possible to prepare zero

* Corresponding author.
E-mail address: skamali@utsi.edu (S. Kamali).
URL: http://www.utsi.edu/ (S. Kamali).

https://doi.org/10.1016/j.jmmm.2017.10.102
0304-8853/

release devices, i. e. deliver drugs by just applying an external stimulus [15,16]. Gated materials with controlled release features have been developed using chemical stimuli [17–21] such as redox molecules, selected anions, pH changes, and biomolecules.

In the authors' recent work [22], a triggered drug release mechanism in mesoporous silica nanoparticles containing magnetic nanocrystallites using an alternating magnetic field was presented.

As low temperature Mössbauer spectroscopy has been shown to be a powerful technique for investigating maghemite nanocrystallites [8,23,24], we used this technique to gain insight into such magnetic nanoparticles and obtain a more accurate estimation of iron distributions.

In this article, we present the formation of such core-shell nanoparticles with γ-Fe_2O_3 nanoparticles as the core and SiO_2 as the shell. The structure and morphology of the nanoparticles were investigated by high-resolution transmission electron microscopy (HR-TEM) and X-ray diffraction (XRD). Energy-dispersive X-ray spectroscopy (EDXS) provides information about the elemental distribution including the incorporation of SiO_2 into the magnetic system. Mössbauer spectroscopy and magnetization measurements were used to gain insight into their magnetic properties as well as the cation distributions. The nature of the magnetic nanoparticles and the morphology of the multi-core nanoparticles are important in medical application such as drug delivery.

In this work multiple single-domain γ-Fe_2O_3 nanoparticles incorporated in a SiO_2 matrix are studied and compared with isolated particles of the same size.

2. Experimental details

2.1. Sample preparation

Iron-oxide nanoparticles were synthesized using a co-precipitation method according to Bruce et al. [25] using 40 mmol iron (III) chloride hexahydrate 97% ($FeCl_3.6H_2O$) and 20 mmol iron (II) chloride tetrahydrate 99% ($FeCl^2.4H^2O$), provided by Sigma–Aldrich, as starting materials. All reagents were used as received. High quality nitrogen gas was employed to create a non-oxidizing atmosphere. For synthesizing the magnetic nanoparticles, 10.80 g iron (III) chloride hexahydrate and 3.97 iron (II) chloride tetrahydrate were first dissolved in 40 mL of de-gasified deionized water and 10 mL of 2.00 mol L^{-1} HCl. The mixture of iron chlorides was poured drop-wise into a round bottomed flask reactor containing 500 mL of a 0.7 mol L^{-1} NH^4OH. A dark brown-black precipitate resulted in this co-precipitation reaction, which continued for 30 min at room temperature and under stirring conditions in an N^2 atmosphere. The particles were separated using a neodymium magnet and the supernatant was removed. To avoid particle agglomeration, 60 mL of a 1 mol L^{-1} tetramethylammonium hydroxide (TMAOH) solution was added and then the volume of the final ferrofluid was adjusted to 320 mL with de-gasified deionized water. The basic ferrofluid was stored at 4 °C under N^2 atmosphere. The magnetic core part, denoted by "core-only" sample, was obtained by drying the ferrofluid at 80 °C.

To synthesize the core shell nanoparticles, denoted from hereon as "multi-core-shell" sample, 1.00 g of a 2.74 mmol hexadecyltrimethylammonium bromide (CTAB) was first dissolved in 480 mL of deionized water. Then, 30 mL of the basic ferrofluid synthesized, as described above, and having a pH of 13 was, added while adjusting the temperature to 80 °C. 5.00 mL of a 22.4 mmol Tetraethylorthosilicate (TEOS) was then added drop-wise to the suspension. After 1 h of stirring, a brown-reddish precipitate was achieved. It was collected by centrifugation and was then washed with deionized water and dried at 70 °C overnight. To prepare the final mesoporous material, the multi-core-shell sample, the as-synthesized solid was calcined at 550 °C in an oxidant atmosphere for 8 h, having a temperature ramp rate of 3 °C/min during the first three hours, to remove the template. More details of the synthesis are presented in the work by Bringas et al. [22].

2.2. XRD

The structure of the nanoparticles was investigated by XRD using a Rigaku Ultima IV diffractometer. A normal line focus CuK_α (λ = 1.5418 Å) radiation tube was used with power settings of 40 kV, 44 mA, and 1.76 kW. Measurements were made using a D/teX Ultra High-Speed Detector with the detector discriminator set in a fluorescent reduction mode. Both samples for a given processing condition were loaded into an automatic rotary sample changer, and diffraction patterns were recorded using a scan speed of 1.00 °/min in a scan range from 10 to 80° $\theta/2\theta$. The raw data were imported into the Integrated X-ray Powder Diffraction Software PDXL package for phase analysis and were compared with the standard patterns in the ICDD database. The PDXL package is also able to perform mathematical fitting based on the Rietveld method.

2.3. HR-TEM and EDXS

The morphology of the synthesized nanoparticles were determined by HR-TEM using a Philips CM12 transmission electron microscope. The average diameter of the nanoparticles was determined by measuring the diameters of 200 particles and fitting the histograms to a Gaussian distribution function.

The EDXS measurements were performed in conjunction with FEI XL30-SFEG scanning electron microscopy operating at a voltage of 5 kV.

2.4. SQUID measurements

Temperature-dependent magnetic susceptibility in the range of 5–350 K in an applied field of 100 Oe, and isothermal magnetization at 5 K and in the range of −20 kOe to 20 kOe were measured with a Quantum Design MPMS-XL SQUID magnetometer.

2.5. Mössbauer spectroscopy

^{57}Fe Mössbauer spectroscopy measurements were performed using an MS4 spectrometer operating in the constant acceleration mode in transmission geometry. The measurements were performed at 10 K using a Janis SVT-400 cryostat. A 100 mCi ^{57}Co in Rh held at room temperature was used as a source. All centroid shifts, δ, are given with respect to metallic α-iron at room temperature. The spectra were least square fitted using Recoil software [26].

3. Results and discussion

3.1. XRD

The XRD spectra for both samples are depicted in Fig. 1. The XRD diffractogram for the core-only sample, shown in the top panel in Fig. 1, has relatively sharp peaks, indicating an excellent crystallinity, evident from (110), (220), (311), (222), (400), (422), (511), (440), and (533) peaks, which are typical for inverse spinel structure nanoparticles [27]. The broadening of the peaks is an indication of the finite size in accordance with the Scherrer equation [28]:

$$d = \frac{\beta\lambda}{B_{1/2}cos(\theta)}. \quad (1)$$

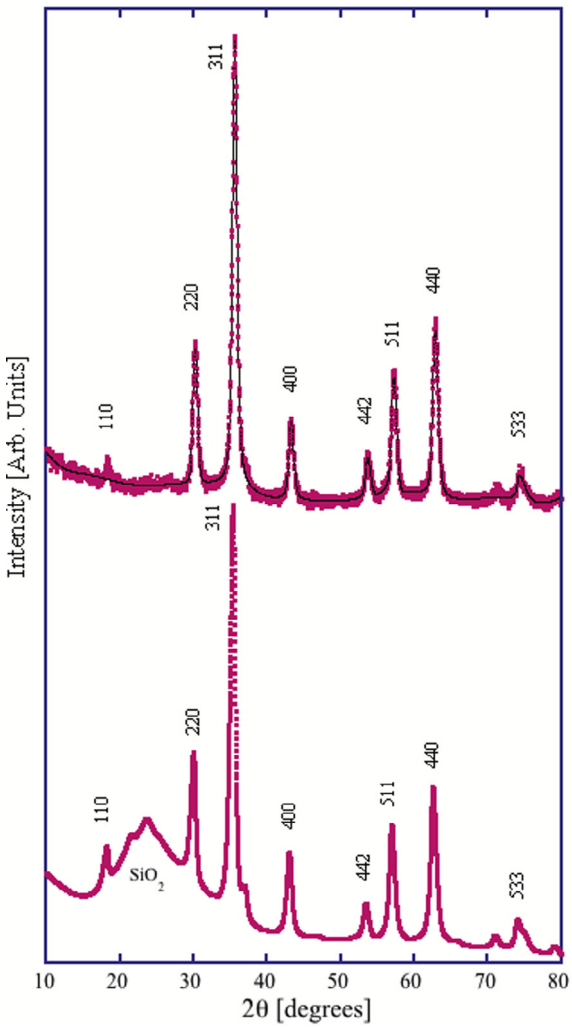

Fig. 1. XRD for the core-only sample (top panel), with the red dots as the experimental data and the solid black line as the fit, and the multi-core-shell sample (bottom panel). The diffraction peaks show clearly that the magnetic core consists of nanoparticles with inverse spinel structure. The broad peak around 24° in the XRD for the multi-core-shell sample (bottom panel), as indicated in the figure, is from the SiO_2.

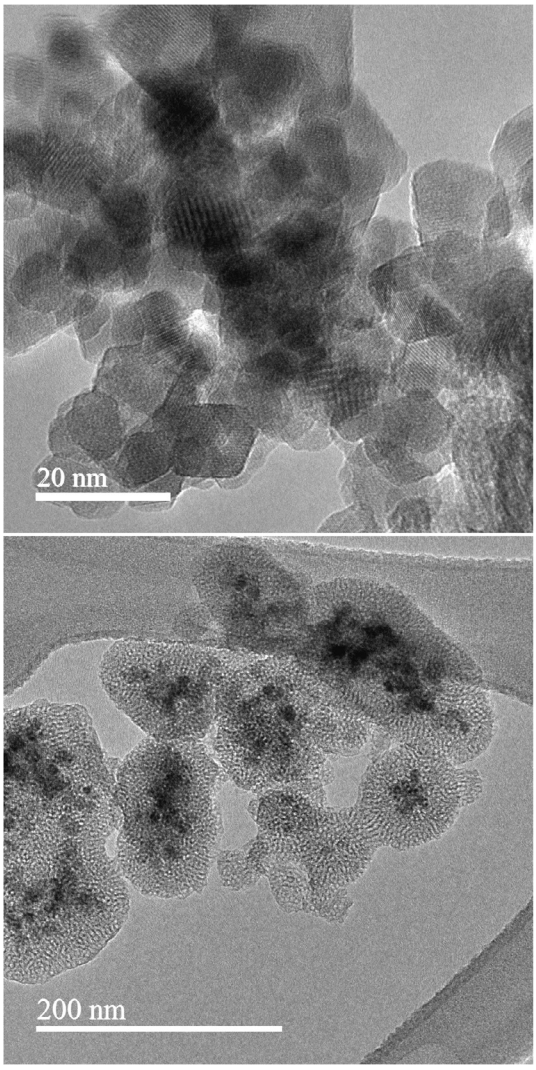

Fig. 2. HR-TEM for the core-only sample (top panel), consisting of spherical γ-Fe_2O_3 nanoparticles, and the multi-core-shell sample (bottom panel) consisting of multiple γ-Fe_2O_3 nanoparticles as the core and silica as the shell. The images have different scales.

where β is 0.94, which is a typical value for cubic structures [29,30], wavelength λ of 1.5418 Å, $B_{1/2}$ is the full width at half maximum (FWHM) of the peaks, and θ is the diffraction angle. FWHM of the instrument is below 0.12° for the whole scanning range, and about one order of magnitude smaller than FWHM refined for the samples for $10 \leqslant 2\theta \leqslant 80°$, thus all peak-broadenings observed for the sample are from the sample and not from the diffractometer. Using the (3 1 1) peak, which has the strongest diffraction, results in a size estimation of 13 nm. The XRD diffractogram for the multi-core-shell sample, shown in the bottom panel in Fig. 1, has the same peaks plus a broad peak around 24°, which is characteristic of the amorphous SiO_2 shell. The reference intensity ratio, the so-called RIR method, reveals that the maghemite/SiO_2 intensity ratio is 32:68.

3.2. HR-TEM

HR-TEM images for both samples are depicted in Fig. 2. As can be seen in Fig. 2 (top panel), the core-only sample consists of spherical nanoparticles with a diameter of 13 ± 2 nm. The core-shell structure is fully formed in the multi-core-shell sample (bottom panel). It should be emphasized that the cores in the multi-core-shell sample consist of several spherical γ-Fe_2O_3 nanoparticles. Furthermore, the EDXS spectra depicted in Fig. 3 show clearly the incorporation of silica into the system for the multi-core-shell sample.

The sample compositions are summarized in Table 1. As can be seen from Table 1, in the multi-core-shell sample, the content of the core, γ-Fe_2O_3, is 33% of the weight, while the shell, SiO_2, has 67% of the weight, in excellent agreement with the XRD results above. These values will be discussed in connection with the magnetization measurements.

3.3. Mössbauer spectroscopy

Mössbauer spectra for both samples are shown in Fig. 4. The hyperfine parameters, magnetic hyperfine field, B_{hf}, magnetic hyperfine distribution, σ, centeroid shift, δ, quadrupole shift, ϵ, and intensity, I, for both samples are summarized in Table 2. The spectrum for the core-only sample consists of an asymmetric sextet. It is best fitted with three components. The first component has a $B_{hf,1}$ of 52.5 T and relatively sharp lines, with a σ_1 of 1.0 T. The

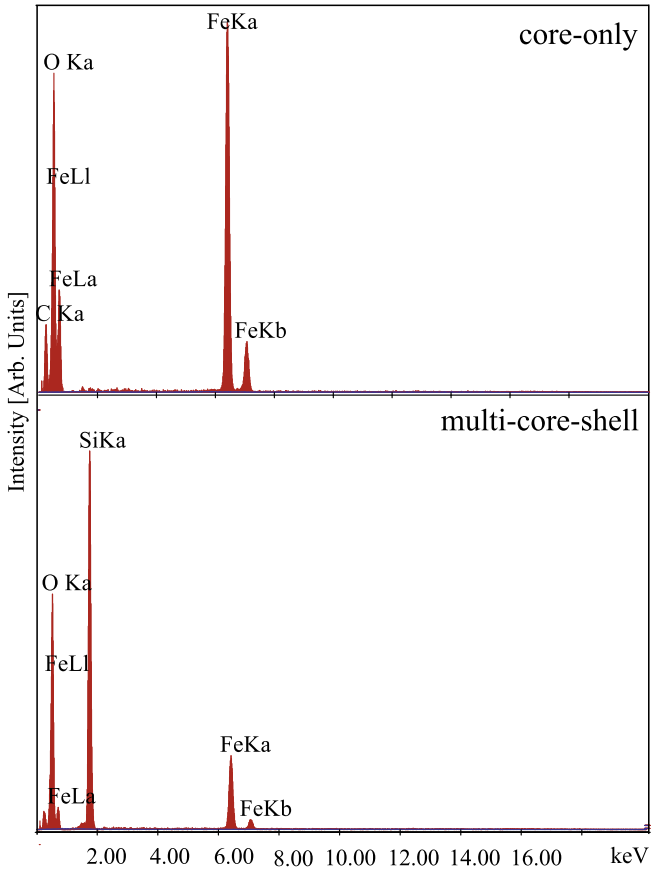

Fig. 3. EDXS for the core-only sample (top panel) and the multi-core-shell sample (bottom panel). The incorporation of SiO_2 is clearly seen in the multi-core-shell sample.

Table 1
Contents of the core, γ-Fe_2O_3, and the shell, SiO_2, extracted from the EDXS measurements

Samples	γ-Fe_2O_3 %	SiO_2 %
Core-only	100	
Multi-core-shell	33	67

relatively high δ value of 0.570 mm/s indicates that this signal is from Fe^{3+} ions in the B-sites. The intensity for this component is 38%. The second sextet has a $B_{hf,2}$ of 52.0 T but much lower δ value, 0.323 mm/s, which is a typical value for Fe^{3+} ions in the A-sites. The third component has slightly lower $B_{hf,3}$ of 49.5 T and δ value of 0.441 mm/s. This signal could also be from Fe^{3+} ions in the B-sites. The reasoning for these assignments will be discussed briefly below. The intensity of 39% for the second component, which is assigned to the A-sites, shows that all cation vacancies, 0.33, are present in the B-sites, and the A-sites are fully occupied. The third component existed in the spectra in the work by Ramos Guivar et al. [31], where it was attributed to the signal from the surface of their nanoparticles due to spin canting effect resulting in a lower B_{hf}. However, the different δ value was not discussed by the authors. A more realistic explanation for this component is that the vacancies in the B-sites result in changes of the volumes of the adjacent cells, which are reflected in a distribution of Fe-O distances. This will partially change B_{hf} and δ values of the B-sites. This is the reason why the third component has a much broader σ_3 of 2.5 T. The spectrum for the multi-core-shell sample is also fitted with three components with almost identical hyperfine parameters. It is worth mentioning that there is no trace of magnetite in these samples [32,33], indicating the magnetic part of these samples is fully oxidized to maghemite.

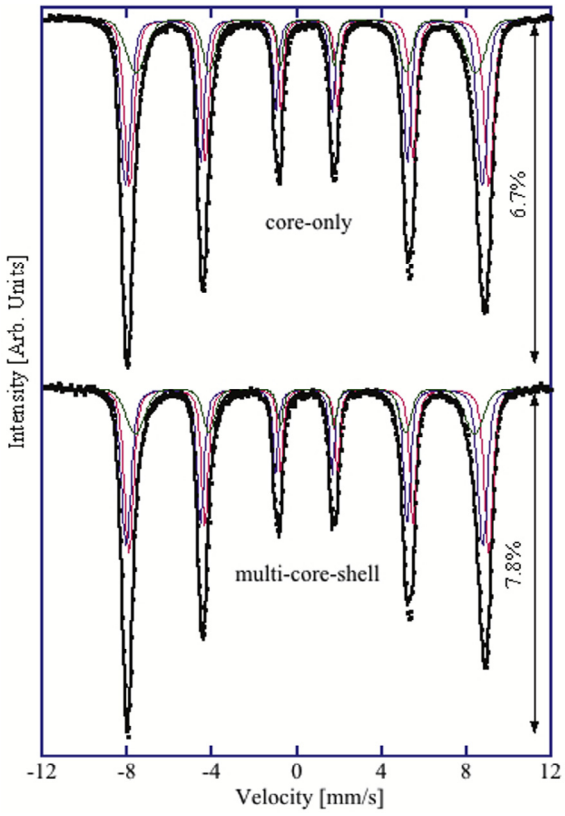

Fig. 4. Mössbauer spectra for both samples measured at 10 K.

Table 2
Hyperfine parameters for both samples: magnetic hyperfine fields (B_{hf}) and their Gaussian distributions (σ), centroid shift (δ), quadrupole shift (ϵ), and intensities (I) of the different components. Estimated errors: ±0.2 T in B_{hf} and σ, ±3% in I, and ±0.002 mm/s in δ and ϵ.

Parameters	core-only	multi-core-shell
$B_{hf,1}$(T)	52.5	52.5
σ_1(T)	1.0	0.9
I_1%	38	39
δ_1(mm/s)	0.570	0.556
ϵ_1(mm/s)	−0.001	−0.003
$B_{hf,2}$(T)	52.0	52.0
σ_2(T)	1.1	1.0
I_2%	39	40
δ_2(mm/s)	0.323	0.330
ϵ_2(mm/s)	−0.002	0.016
$B_{hf,3}$(T)	49.5	49.4
σ_3(T)	2.5	2.4
I_3%	23	21
δ_3(mm/s)	0.441	0.415
ϵ_3(mm/s)	−0.040	−0.055

3.4. Magnetization measurements

The isothermal magnetization hysteresis loops for both samples are depicted in Fig. 5. The saturation magnetization, M_s, the remanence, M_r, and the coercive field, B_c values for both samples are summarized in Table 3. As can be seen in Table 3, the M_s for the core-only sample is 80.35 emu/g, while it is 27.11 emu/g for the

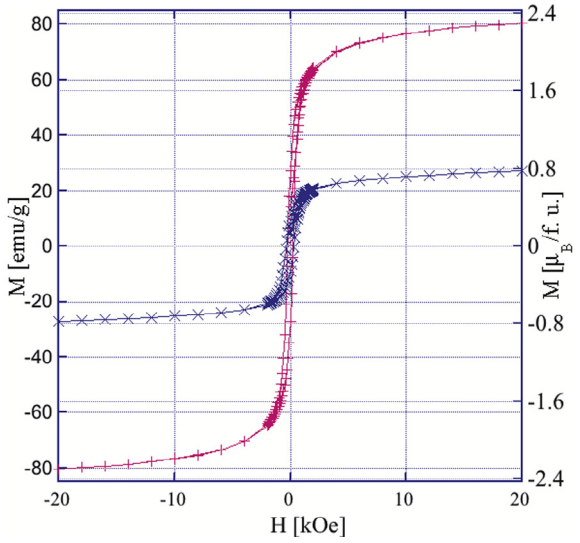

Fig. 5. Isothermal magnetization hysteresis loops at 5 K for the core-only sample (+) and for the multi-core-shell sample (×).

Table 3
Saturation magnetization, M_s, remanence, M_r, and coercive field, B_c, for both samples extracted from the isothermal magnetization measurements.

Samples	Composition	M_s emu/g	M_r emu/g	B_c Oe
Core-only	γ-Fe_2O_3 only	80.35	27.32	500
Multi-core-shell	γ-Fe_2O_3@SiO_2	27.11	9.17	670

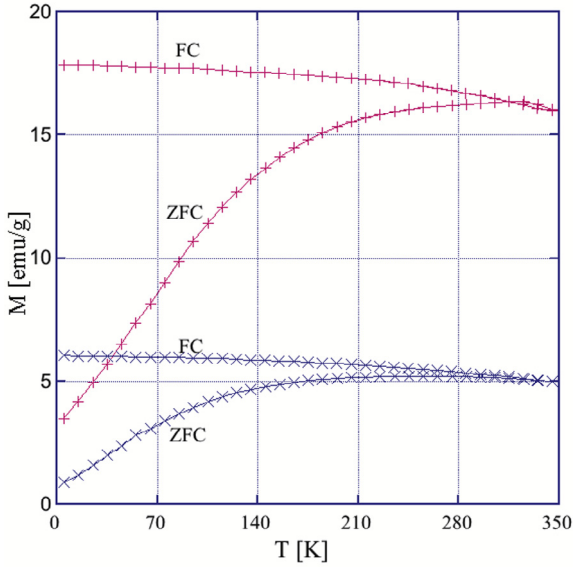

Fig. 6. ZFC and FC measurements in the temperature interval of 5–350 K in an applied field of 100 Oe for the core-only sample (+) and for the multi-core-shell sample (×).

multi-core-shell sample, in accordance with the γ-Fe_2O_3 to SiO_2 ratio from the EDXS results. The M_r values also follow the γ-Fe_2O_3 to SiO_2 mass ratios from the EDXS results. The B_c values at 5 K for both samples are very close to each other, around 600 Oe. At higher temperatures they will be much lower and above the blocking temperature they will be zero in the superparamagnetic state.

As the core-only sample consists of magnetic nanoparticles only, it would be interesting to depict the magnetization in μ_B per formula unit for this sample. The right-side y-axis of Fig. 5 shows the magnetization in μ_B per formula unit. The core-only sample has an M_s of 2.30 μ_B per formula unit.

Fig. 6 shows the zero-field-cooled (ZFC) and field-cooled (FC) magnetization measurements in the temperature range of 5–350 K in an applied field of 100 Oe. Similar to the isothermal magnetization measurements the magnetization for the core-only sample is much higher than for the multi-core-shell sample, while both samples show blocking temperature around the room temperature.

4. Conclusions

In this study, the magnetic properties and the formation of a multi-core sample having 13 nm γ-Fe_2O_3 nanoparticles as the core and silica as the shell have been investigated by means of various techniques. Low temperature Mössbauer spectroscopy reveals the presence of γ-Fe_2O_3 as the magnetic nanoparticles. The multiple-core γ-Fe_2O_3 nanoparticles and the isolated particles of the same size show similar behaviors. Zero-field-cooled and field-cooled measurements and isothermal magnetization results are in agreement with the constituents being a magnetic core and the shell being non-magnetic. The HR-TEM images corroborate the formation of a core-shell structure.

Acknowledgements

We thank the assistance by Dr. Peter Klavins at the Department of Physics, the University of California Davis, in performing the magnetization measurements. This research was partially supported by the Department of Energy, Office of Nuclear Energy, Nuclear Energy Program, under Grant No. DE-NE0000704.

Appendix A. Supplementary data

Supplementary data associated with this article can be found, in the online version, at https://doi.org/10.1016/j.jmmm.2017.10.102.

References

[1] J. Fidler, T. Schrefl, W. Scholz, D. Suess, V.D. Tsiantos, R. Dittrich, M. Kirschneret, Physica B: Condenced Matter 343 (2004) 200.
[2] S. Sun, C.B. Murray, J. Appl. Phys. 85 (1999) 4325.
[3] B.A. Holm, E.J. Bergey, T. De, D.J. Rodman, R. Kapoor, L. Levy, C.S. Friend, P.N. Prasad, Mol. Cryst. Mol. Liquids 374 (2002) 589.
[4] R. Hergt, W. Andra, C.G. d'Ambly, I. Hilger, W.A. Kaiser, U. Richter, H.G. Schmidt, IEEE Trans. Magn. 34 (1998) 3745.
[5] J.H. Gao, H.W. Gu, B. Xu, Acc. Chem. Res. 42 (2009) 1097.
[6] J. Tucek, R. Zboril, D. Petridis, J. Nanosci. Nanotechnol. 6 (2006) 926.
[7] S. Mørup, J. Magn. Magn. Mater. 37 (1983) 39.
[8] S. Kamali-M, T. Ericsson, R. Wäppling, Thin Solid Films 515 (2006) 721.
[9] A.A. Jordan, P. Wust, R. Scholz, et al., in: U. Häfeli, W. Schütt, J. Teller, M.Z. (Eds.), Plenum Press, New York, 1997.
[10] M.D. Cuyper, M. Joniau, Eur. Biophys. J. 15 (1988) 311.
[11] M.D. Cuyper, P. Müller, H. Lueken, M. Hodenius, J. Phys.: Condens. Matter 15 (2003) 1425.
[12] A. Ulrich, Biosci. Rep. 22 (2002) 129.
[13] F. Jähnig, Biophys. J. 46 (1984) 687.
[14] J. Hernandez-Borrell, F. Mas, J. Puy, Biophys. Chem. 36 (1990) 47.
[15] E. Aznar, R. Martinez-Máñez, F. Sancenón, Expert Opin. Drug Delivery 6 (2009) 643.
[16] K. Cotí, M.E. Belowich, M. Liong, M.W. Ambrogio, Y.A. Lau, H.A. Khatib, J.I. Zink, N.M. Khashab, J.F. Stoddart, Nanoscale 1 (2009) 16.
[17] C.Y. Lai, B.G. Trewyn, D.M. Jeftinija, K. Jeftinija, S. Xu, S. Jeftinija, V.S.Y. Lin, J. Am. Chem. Soc. 125 (2003) 4451.
[18] C. Park, K. Oh, S.C. Lee, C. Kim, Angew. Chem., Int. Ed 46 (2007) 1455.
[19] R. Casasús, E. Climent, M.D. Marcos, R. Martinez-Máñez, F. Sancenón, J. Soto, P. Amorós, J. Cano, E. Ruiz, J. Am. Chem. Soc. 130 (2008) 1903.
[20] R. Liu, P. Liao, J. Liu, P. Feng, Langmuir 27 (2011) 3095.
[21] E. Climent, R. Martinez-Máñez, F. Sancenón, M.D. Marcos, J. Soto, A. Maquieira, P. Amorós, Angew. Chem., Int. Ed. 49 (2010) 7281.

[22] E. Bringas, ÖKöysüren, D.V. Quach, M. Mahmoudi, E. Aznar, J.D. Roehling, M.D. Marcos, R. Martinez-Máñez, P. Stroeve, Chem. Commun. 48 (2012) 5647.
[23] L. Häggström, S. Kamali, T. Ericsson, P. Nordblad, A. Ahniyaz, L. Bergström, Hyperfine Interact. 183 (2008) 49.
[24] A. Ahniyaz, G.A. Seisenbaeva, L. Häggström, S. Kamali, V.G. Kessler, P. Nordblad, C. Johansson, L. Bergström, J. Magn. Magn. Mater. 320 (2008) 781.
[25] I.J. Bruce, J. Taylor, M. Todd, M.J. Davies, E. Borioni, C. Sangregorio, T. Sen, J. Magn. Magn. Mater. 284 (2010) 145.
[26] K. Lagarec, D. Rancourt, Recoil, Mössbauer spectral analysis software for Windows, version 1.0, 1998.
[27] S. Mahadevan, G. Gnanaprakash, J. Philip, B.P.C. Rao, T. Jayakumar, Physica E 39 (2007) 20.
[28] B.D. Cullity, S.R. Stock, 3 ed., Elements of X-Ray Diffraction, Prentice-Hall Inc., 2001.
[29] H.P. Klug, L.E. Alexander, X-Ray Diffraction Procedures: For Polycrystalline and Amorphous Materials, 2nd ed., Wiley-Interscience, 1974.
[30] J.I. Wang, I.R. Harrison, In Polymers, Part B: Crystal Structure and Morphology. Methods of Experimental Physics, Academic Press, 1980.
[31] J.A. Ramos-Guivar, E.A. Sanches, F. Bruns, E. Sadrollahi, M.A. Morales, E.O. López, F.J. Litterst, Appl. Surf. Sci. 389 (2016) 721.
[32] L. Häggström, H. Annersten, T. Ericsson, R.L. Wäppling, W. Karner, S. Bjarman, Hyperfine Interact. 5 (1978) 201.
[33] F.J. Berry, S. Skinner, M.F. Thomas, J. Phys.: Condens. Matter 10 (1998) 215.